MAUSAM, 48, 2 (April 1997), 135-156

551.515.2 : 551.558.1

Impact of parameterized convection on a numerically simulated tropical cyclone structure

MUKUT B. MATHUR

National Center for Environmental Prediction, Washington D.C.

सार — उष्णकटिबंधीय चक्रवात जैसे विक्षोभों के लिए संघनन-ऊष्मा ऊर्जा का मुख्य स्रोत है। बारीक जाली से बने अनेक गणितीय निदर्श, जिनका प्रयोग गतिक प्रक्रियाओं के आकलन के लिए किया जाता है, इनमें विभेद्य स्केल संघनन तथा प्राचलिक संवहन का मूल्यांकन काल-खंडों की अपेक्षा लम्बे अंतरालों में मिनटों में किया जाता है। पृच्छन्न ऊष्मन, निदर्श विभेदन तथा वर्षण भौतिकी के मूल्यांकन के अंतराल पर निर्भर करता है। क्षैतिज विभेदन में परिवर्तन और संघनन भौतिकी के मूल्यांकन के अंतराल तथा प्राचलिक संवहन ऊष्मा के निवारण के प्रभाव का अध्ययन करने के लिए अल्पावधि पूर्वानुमानों की ऋंखला के प्राप्त गणितीय परिणामों की तुलना की जाती है। राष्ट्रीय पर्यावरणीय पूर्वानुमान केन्द्र के क्वासी-लागरेंजन निदर्श (क्यू.एल.एम. तथा उष्णकटिबंधीय चक्रवात के मामलों के आरम्भिक आकड़ों का 40 कि.मी. (मोटी जाली) अथवा 20 कि. मी. (बारीक जाली) वाले क्षैतिज ग्रिड अंतरण में उपयोग किया गया है। अतिसंतृप्त ग्रिड केन्द्रों में ही विभेद्य स्केल संघनन का उपयोग किया गया है, और एक कुओ-टाइप संवहनीय प्राचलिक पद्धति का उपयोग किया गया है।

जब प्राचलिक संवहन और विभेद्य स्केल दोनों के आकलन के अंतराल में परिवर्तन किया जाता है, तब महत्वपूर्ण संरचनात्मक भिन्नताएँ उत्पन्न होती हैं और क्षैतिज विभेदन में वृद्धि के साथ ये भिन्नताएँ और भी अधिक बढ़ जाती है। जब दोनों संघनन प्रक्रियाओं का मूल्यांकन प्रत्येक काल-खंड के बजाय बारह काल-खंडों के अंतराल पर किया जाता है, तब केन्द्रीय तापन क्रोड संरचना और चक्रवातीय तीव्रता में सुसंगति पाई जाती है। जब दोनों संघनन प्रक्रियाएँ प्रत्येक काल-खंड पर की जाती हैं, तब चक्रवात के मध्य क्षेत्र में उर्ध्वाधर वायु पुंज संवहनी रूप से तीव्र गति से स्थिर हो जाते हैं, और अधिकतम उर्ध्वाधर रुख की तथा क्षैतिज प्रबल पवनें चक्रवात के बाहरी क्षेत्र की ओर बढ़ जाती हैं। जब दोनों संघनन प्रक्रियाओं का मानांकन बारह काल-खंडों के अंतराल पर किया जाता है तब चक्रवात का केन्द्रीय क्षेत्र अस्थिर रहता है और प्रबल पवनें केन्द्र की ओर बढ़ जाती है।

बारीक जाली के प्रयोग में भी चक्रवात का केन्द्रीय क्षेत्र परिस्थिति के अनुसार अस्थिर रहता है, जिसमें प्राचलिक संवहनीय ऊष्मन, को उपयोग में नहीं लाया जाता है और विभेद्य स्केल ऊष्मन का मूल्यांकन प्रत्येक काल-खंड में किया जाता है। उर्ध्वाधर सघन पवन पुंजों में उर्ध्वाधर तीव्र गति और प्रबल ऊष्मन उत्पन्न होता है, जिससे इस तथ्य का पता चलता है कि संवहनीय पैमाने में ऊष्मन, विभेद्य पैमाने के ऊष्मन के अनुरूप होता है। इस मामले में पहले 6 घंटों के दौरान, ऊष्मन का उर्ध्वाधर वितरण और चक्रवातीय संरचना, बारीक जाली वाले प्रयोग के समान पाई गई है जिसमें दोनों संघनन प्रक्रियाओं का मूल्यांकन बारह काल-खंडों के अंतराल पर किया जाता है। तथापि, बाद के मामले की तुलना में पहले के मामलों में तूफान छः घंटे के बाद अधिक तेजी से प्रबल होता है। और अधिक अग्रिम प्रयोगों से प्राप्त गणितीय परिणाम यहाँ पर यह दर्शाने के लिए दिए गए हैं कि एक अथवा दोनों संघनन प्रक्रियाओं के सक्रिय करने के अंतराल में परिवर्तन के अनुसार पूर्वानुमानित चक्रवात संरचना में परिवर्तन होता है, और ये परिचालन परिवर्तन आरम्भिक प्रक्रिया के कारण नहीं होते हैं।

कपासी-वर्षा मेघों में नमी और ऊष्मा निम्न स्तरों में उच्च क्षोभमंडल में कई मिनटों में पहुँच जाती है। उपरोक्त और क्यू.एल.एस. से प्राप्त अन्य पूर्वानुमानों से ज्ञात होता है कि यदि प्राचलिक संवहनीय ऊष्मन को शामिल किया जाए तो मेसोस्केल निदर्श में तूफान संरचना, तीव्रता और गति में सुधार आ सकता है; तथापि, प्राचलीकरण स्कीम को कई मिनटों के अंतराल पर सक्रिय किया जाना चाहिए, जिससे समूचे निदर्श में मेघ सघनता में होने वाले परिवर्तनों का उनके साथ-साथ पता चलता है।

ABSTRACT. Condensational heating is a primary source of energy for disturbances like a tropical storm. The resolvable scale condensation and the parameterized convection, in many fine mesh numerical models, are evaluated at intervals greater than the time step, order of a minute, used for computing dynamical processes. The latent heating may depend on the model resolution and the interval at which the precipitation physics is evaluated. Numerical results from a series of short range forecasts are compared to study the impact of varying the horizontal resolution and the interval for evaluating condensation physics, and of excluding the parameterized convective heating. A horizontal grid spacing of 40 km (coarse mesh) or 20 km (fine mesh) in National Centers for Environmental Prediction's Quasi-Lagrangian Model (QLM), and the initial data for a tropical storm case, are utilized. Resolvable scale condensation is invoked only at supersaturated grid points, and a Kuo-type convective parameterization procedure is employed.

Significant structural differences are produced when the interval for computing both parameterized convection and resolvable scale heating is changed, and these differences broaden when the horizontal resolution is increased. The central warm core structure and storm intensity are simulated better when both condensational processes are evaluated at an interval of twelve time steps than at each time step. Vertical columns in central storm area rapidly become convectively stable, and the maximum in vertical motion and strogest horizontal winds shift in the outer storm area, when both condensational processes are invoked at each time step. The central storm area remains conditionally unstable, and strongest winds develop close to the center, when both condensational processes are evaluated at intervals of twelve time steps.

The central storm area remains conditionally unstable also in the fine mesh experiment in which the parameterized convective heating is excluded and the resolvable scale heating is evaluated at each time step. Intense vertical motion and vigorous heating develop in deep vertical columns, indicating that the heating on the convective scale is simulated as the resolvable scale heating. The vertical distribution of heating and the storm structure, during the first six hours in this case, are similar to those in the fine mesh run in which both condensational processes are evaluated at intervals of twelve time steps. However, the storm intensifies more rapidly after 6 h in the former than in the later case. Numerical results from additional experiments are presented to show that predicted storm structure is modified with a change in interval for invoking either or both condensational processes, and these circulation differences are not due to the initial spin up.

Transfer of moisture and heat from low levels into the higher troposphere in cumulonimbus clouds takes place in several minutes. Above cited and other predictions from the QLM suggest that storm structure, intensity and motion in a mesoscale model are likely to be improved when parameterized convective heating is included; however, a parameterization scheme that concurrently produces alterations in the entire model cloud depth should be invoked at intervals of several minutes.

Key words — Parameterized convection, Equivalent potential temperature, Pressure gradient, Condensational heating, Instability, Vertical motion.

1. Introduction

Condensational release of latent heat is a main source of energy for low latitude disturbances, and this heating is essential for the development of tropical cyclones. In many numerical models the phase change, vapour to water, may occur in the following two forms:

(1) *Grid scale or resolvable scale condensation* — If a layer is supersaturated then the excess moisture is condensed. The adjustment of the temperature and moisture is usually carried out so that the layer relative humidity is 100% after the condensation. This condensation process is often referred to as the isobaric release of latent heat (since the pressure in the adjusted layer is assumed to remain constant during the adjustment), or the large scale release of latent heat because supersaturation often occurs due to large scale processes such as the advection of moisture and temperature). The temperature and moisture in only the supersaturated layer is adjusted in this process. However, in some models if a layer below the adjusted layer is unsaturated, then the rain falling into such a lower layer is allowed to evaporate until either this layer becomes saturated or all falling rain is evaporated (Mathur 1991). Thus the thermodynamic state in a column below the supersaturated layer may be changed.

TABLE 1

List of experiments. Interval at which the parameterized convective heating (CI) and the resolvable condensation (RI) are invoked is given as a multiple of the time step. A time step of 50s is used in the coarse (40 km), and 40s in the fine (20 km), horizontal resolution experiments. Convective parameterization scheme based on Kuo (1965) is utilized in all experiments except G20L12B and G20L01B, where the scheme based on Kuo (1974) is used.

EXPERIMENT	GRID	VERTICAL SPACING LAYERS	LATENT HEAT		CI	RI
			CONVECTIVE	RESOLVABLE		
Case: Hurricane Bob. Initial time : 0000 UTC 17 August 1991						
G40L12	40 km	16	yes	yes	12	12
G40L01	40 km	16	yes	yes	1	1
G20L12	20 km	10	yes	yes	12	12
G20L01	20 km	10	yes	yes	1	1
G20NC1	20 km	10	no	yes		1
Ancillary Experiments						
G20L15	20 km	10	yes	yes	15	15
G20C12R1	20 km	10	yes	yes	12	1
G20L12L1	20 km	10	yes	yes	Both processes evaluated at intervals of 12 time steps during the first 6 hours and then at each time step.	
G20L1L12	20 km	10	yes	yes	Both processes evaluated at each time step during the first 6 hours and then at intervals of 12 time steps.	
G20L12B	20 km	10	yes	yes	12	12
G20L01B	20 km	10	yes	yes	1	1
Case : Hurricane Andrew, Initial time 1200 UTC 23 August 1992						
A40L12	40 km	16	yes	yes	12	12
A40L01	40 km	16	yes	yes	1	1

(2) *Subgrid-scale or convective condensation* — The release of latent heat occurs in the form of convective clouds in a conditionally unstable column. In many operational models, the horizontal grid spacing is much greater than the horizontal dimension of convective clouds (a few kilometres), and this release of latent heat is evaluated using a parameterization procedure. The model convective clouds are assumed usually to have their bases in the boundary layer.

The evaluation of condensational processes entails considerable computational time. Therefore, the precipitation physics is invoked, in some operational models of the National Centers for Environmental Prediction (NCEP), at intervals greater than the time step that is used for calculating other terms (like advection). As an example, the convective (resolvable scale) release of latent heat is evaluated at every fourth (second) time step in NCEP's ETA model (Janji'c 1990, Mesinger *et al.*, 1988). Two grids are currently used in NCEP's Nested Grid Model (NGM) of Philips (1979). Both latent heats are invoked at 15 minute intervals, while a time step of 90s (180 s) is used in the inner (outer) mesh.

It is likely that the predicted circulation depends on the interval at which the physical forcing, the condensational heating, it evaluated. It is also generally recognized that more intense vertical motion and condensational heating are often produced when the resolution of a model is increased. In this paper, we discuss a series of integrations for a hurricane Bob case (initial time 0000 UTC 17 August 1991) varying the model resolution, interval for evaluating condensational heating, and with the exclusion of the

parameterized convection. Bob was a tropical storm (central pressure 1005 hPa) at the above initial time and it intensified into a hurricane during the next 24 hours.

Experiments are carried out using NCEP's Quasi-Lagrangian Model (QLM), and the resolution and the time step used in the QLM integrations are provided in Table 1. The QLM is a limited-area model; an overview of the QLM and the design of experiments is given in section 2. We show in section 3, that the location and the vertical distribution of condensational heating are modified when the interval for evaluating condensational heating is changed; the forecast storm structure, and motion are predicted better when the condensational physics is evaluated at an interval of twelve time steps than at each time step. Furthermore, the differences in forecast with the change in interval for evaluating condensation become more pronounced when the horizontal resolution is increased.

The results from the integration of the QLM with the exclusion of the parameterized convection and the evaluation of the large scale condensation at each time step, are described in section 4; the forecast circulation is much weaker with than without the inclusion of the parameterized convection. Results from additional experiments are presented in section 5 to elucidate further the impact, on predicted storm structure and of changing the horizontal resolution and the interval for evaluating either condensation processes. A summary of our results and conclusions are given in section 6.

2. Experimental setup

The QLM is a primitive equation model with σ (= pressure / surface pressure) as the vertical coordinate. The two horizontal components of the wind, the potential temperature, the mixing ratio, and the surface pressure are predicted using a quasi-Lagrangian scheme (Mathur 1983, 1991). The vertical motion is diagnosed from the integration of the pressure tendency equation. Parameterized convection as well as the resolvable scale release of latent heat are included. The resolvable scale condensation is evaluated at supersaturated grid points and the evaporation of rain falling into the lower layers, mentioned in section 1, is included. The temperature and mixing ratio in the model convective cloud are taken as those along the pseudo-adiabat through the lifting condensation level (LCL) of the parcel from the lowest model layer. If the model convective cloud is warmer and more moist than the environment in at least two layers above the LCL, then the heating and moistening of such environmental layers is carried out based on Kuo (1965).

The data on the QLM grid are derived by interpolation of NCEP's global Aviation analysis (Parrish and Derber 1992). The Aviation analysis has a resolution of about 100 km. Because of lack of data, a storm's circulation is not resolved well in the Aviation analysis. For improving the initial storm structure, an idealized circulation representing the observed storm is merged into the QLM gridded data. The idealized circulation is a combination of an idealized vortex in gradient balance whose size and intensity match those of the observed storm, and a steering current based on storm's current motion (Mathur 1991). Both the structure and motion of a storm is predicted better with than without the inclusion of the idealized circulation in the analysis; the QLM forecast track errors have been the smallest among operational forecast track models in many Atlantic Ocean storm cases (Mathur 1991, Mathur and Ruess 1993).

A 16-layer QLM with the grid spacing of 40 km (coarse mesh), and a 10-layer QLM with the grid spacing of 20 km (fine mesh) are utilized in this study (see Table 1 for a list of experiments). A domain of roughly 4400 × 4400 km is used. Because of computational constraints we used, a lower vertical resolution in the fine mesh QLM. In an earlier paper (Mathur 1992), it is shown that the impact on forecasts is much greater with the increase in horizontal resolution than that with the decrease of the vertical resolution. A time step of 50 s (40 s) issued in the coarse (fine) mesh integration. Strongest pressure gradients in many hurricanes occur within 10-50 km from the center. The strong pressure gradients near the center cannot be resolved with the horizontal resolution utilized in the QLM; the maximum pressure gradients in the QLM idealized vortex and initial state are often located at distances greater than 50 km from the center.

3. Predictions with the parameterized convection

Coarse, and fine, mesh QLM integrations with the parameterized convection (based on Kuo 1965 scheme) and the resolvable scale release of latent heat evaluated at each, or at every twelfth, time step are compared in this section. It is shown below that dissimilarities in the two high horizontal resolution (20 km) runs are greater than in the two low horizontal resolution (40 km) experiments. The maximum vorticity center at 850 hPa in the storm area is taken as the center of the

storm in our study, and the storm center nearly coincides with the center of the area shown in figures. The observed and predicted locations of the storm center in the main experiments described in this and the following section are given in Table 2.

(a) *Use of a low horizontal resolution (grid spacing of 40 km)*

It is shown below that by 24 h, the warm core structure, large upward motion and strong horizontal winds occur near the storm center, when an interval of twelve time steps for evaluating the condensational physics is used (experiment G40L12). The warm core is weaker, and the areas with strong horizontal winds and large upward motion shift far from the center, when the condensational physics is evaluated at each time step (experiment G40L01). Significant differences in G40L12 and G40L01 that appear by 24 h are discussed in the following.

(1) *Horizontal structure*

(*i*) *Pressure distribution* — During the first 12 h, the central mean sea level pressure in G40L12 and G40L01 is nearly the same, by the innermost isobar occupies a larger area in G40L01 (not shown). A deeper storm develops in G40L12 than in G40L01 by 24 h. The mean sea level pressure is 994 hPa in G40L12 (Fig. 1a) and 998 hPa in G40L01 (Fig. 1b). The central pressure at 24 h was somewhat closer to the observed (982 hPa) in G40L12 than in G40L01.

The size of the storm is smaller in G40L12 than in G40L01. In this regard, note that closed isobars in storm's outer region (e.g. 1008 and 1012 hPa) occupy larger areas in G40L01 than in G40L12. The horizontal pressure gradients at 850 hPa near the center are much stronger in G40L12 (Fig. 1c) than in G40L01 (Fig. 1d). The maximum pressure gradient is located farther from the center in G40L01 than in G40L12; the maximum value in G40L12 (50 ms^{-1} h^{-1}) develops to the southeast of the center, while the maximum in G40L01 (30 ms^{-1} h^{-1}) appears to the northeast of the center. The pressure gradients within 100 km from the center are much stronger (weaker) in G40L12 (G40L01) to the east than to the west of the center.

(*ii*) *Low level circulation* — The 850 hPa maximum wind is located within 150 km to the east of the center during the first 12 hours in both G40L12 and G40L01, but the winds are somewhat stronger in G40L01 (not shown). The maximum wind at 24 h is located farther from the center and is weaker in G40L01 than in G40L12 (Fig. 2). These difference in the strength and location of the maximum wind at 24 h are related to the development of the maximum pressure gradient that is weaker and is located farther from the center in G40L01 than in G40L12 (Fig. 1). Also notice that the storm center in G40L01 is situated to the northeast of its position in G40L12. The displacement of the vortex in the first 24 h is closer to the observed in G40L12 than in G40L01 (see Table 2).

TABLE 2

A comparison of forecast intensity (central pressure in hPa) and location (latitude/longitude of the storm center) in coarse (40 km), and fine (20 km), mesh experiments.

	Forecast intensity		Forecast location	
Experiment	12 hr	24 hr	12 hr	24 hr
OBSERVATIONS	996	982	28.3°N 76.9°W	29.6°N 77.3°W
G40L12	1007	994	28.8°N 76.6°W	31.2°N 76.8°W
G40L01	1007	998	29.4°N 76.9°W	31.5°N 76.4°W
G20L12	996	976	28.2°N 76.7°W	30.5°N 76.6°W
G20L01	1001	989	27.9°N 76.4°W	32.2°N 76.0°W
G20NC1	992	970	27.8°N 76.5°W	29.9°N 77.0°W

(*iii*) *Conditional instability* — The mean tropical atmosphere is known to be conditionally unstable in the lower troposphere and stable in the upper troposphere, i.e., the equivalent potential temperature θ_e decreases (increases) with height in the lower (upper) troposphere. This thermodynamic structure is modified in the regions where the vertical transport of heat and moisture takes place mainly in the form of convective clouds. The distribution of $\partial\theta_e / \partial p$ at a low tropospheric layer (900 hPa) at 6 h and 24 h in G40L12 and G40L01 is shown in Fig. 3. At the initial time, $\partial\theta_e / \partial p$ was about 18 × 10^{-3} °K hPa^{-1} at the storm center with larger values away from the center (30 × 10^{-3} °K hPa^{-1} at the periphery of the storm). During the first 6 h, $\partial\theta_e / \partial p$ increases (decreases) over the central storm area in G40L12 (G40L01). The storm's central area becomes stable in G40L01 (Fig. 3b) and more conditionally unstable (that at the initial time) in G40L12 (Fig. 3a). Notice also that high

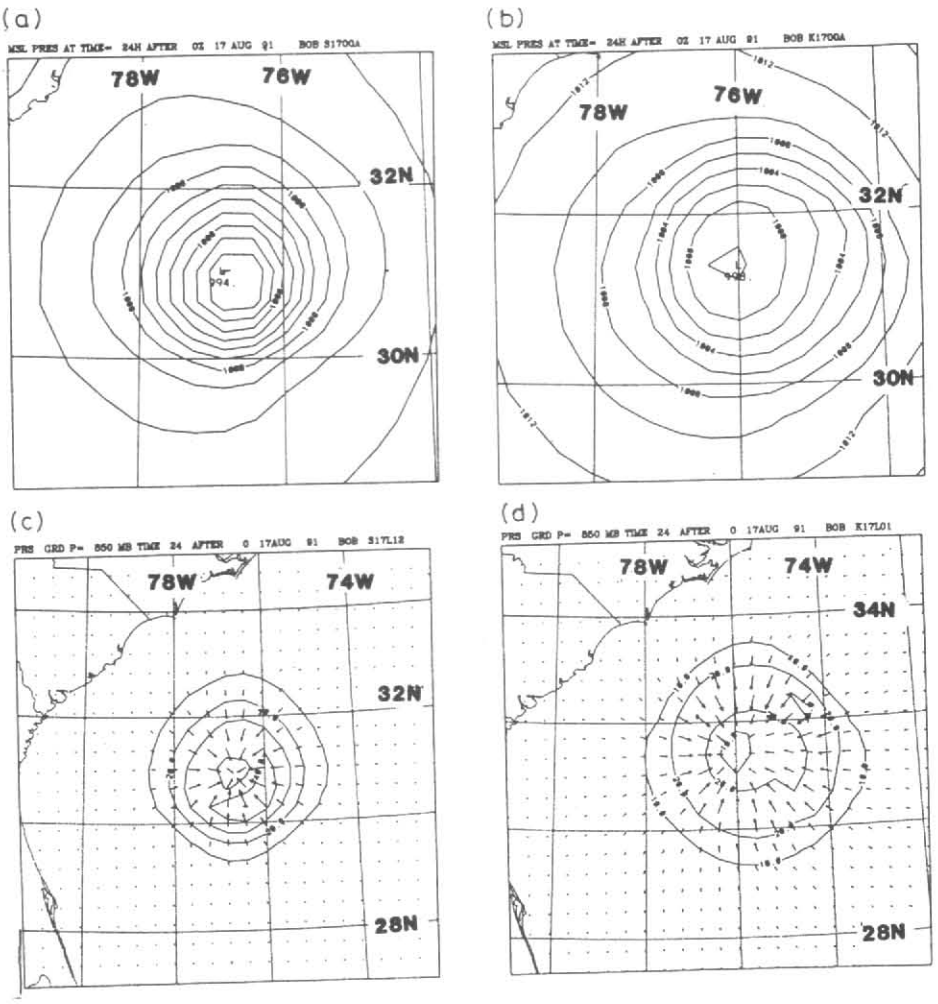

Figs. 1(a-d). Forecast fields in the storm area at 24 h after 0000 UTC 17 August 1991. Mean sea level pressure hPa (a) experiment G40L12 and (b) experiment G40L01. Pressure gradient ($ms^{-1}h^{-1}$) at 850 hPa: (c) experiment G40L12 and (d) experiment G40L01. See Table 1 for a list of experiments

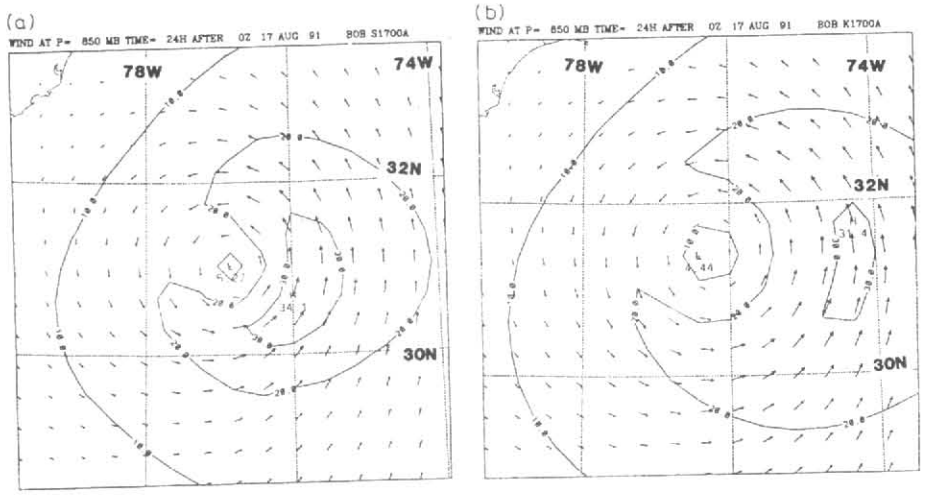

Figs. 2(a-b). Forecast 850 hPa winds in the storm area at 24 h after 0000 UTC 17 August 1991: (a) experiment G40L12 and (b) experiment G40L01. Isotachs are drawn at 10 ms^{-1} intervals. See Table 1 for a list of experiments

and low values of $\partial\theta_e / \partial p$ occur at 6 h in both experiments at nearly the same locations at 200-400 km to the east and to the west of the center. At 24 h, the lower troposphere is nearly stable in

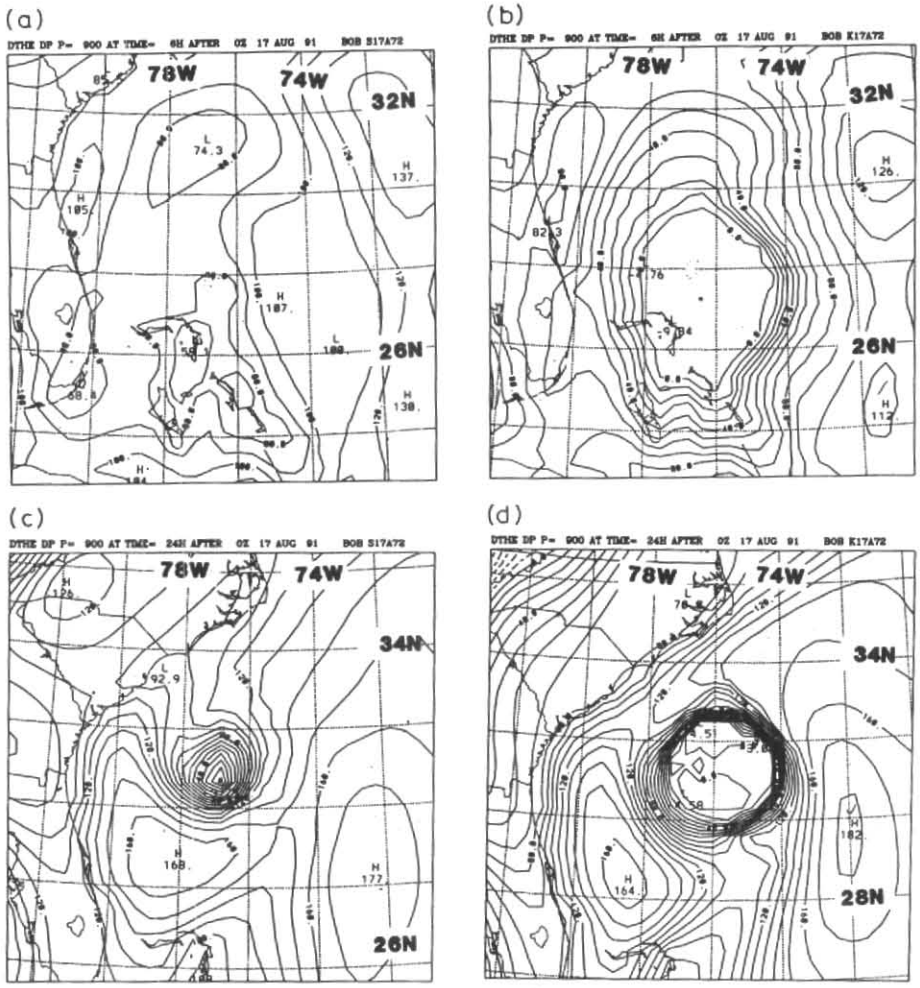

Figs. 3(a-d). Distribution of $\partial \theta_e / \partial p$ (10^{-3} °K hPa^{-1}) at 6 h in (a) experiment G40L12 and (b) experiment G40L01; at 24 h in (c) experiment G40L12 and (d) experiment G40L01. The initial time for the forecasts is 0000 UTC 17 August 1991. See Table 1 for a list of experiments

the central storm area in G40L01 with large gradients in $\partial\theta_e$ / ∂p at about 100 km from the center (Fig. 3d). Negative values of $\partial\theta_e$ / ∂p appear in a very small area near the center, and $\partial\theta_e$ / ∂p increases rapidly away from the center in G40L12 (Fig. 3c). Thus, the structure of $\partial\theta_e$ / ∂p in G40L12 and G40L01 is disparate in central storm area, and it is similar in the storm's environment.

(2) *Vertical structure*

The cross sections in this paper are drawn through the grid point closest to the center of the storm. The west to east cross sections for the vertical motion, equivalent potential temperature, potential temperature and tangential velocity at 24 h in G40L12 and G40L01 are shown in Fig. 4. The vertical structure in G40L12 is quite different from that in G40L01. Large upward motion in a deep column develops above the central storm area in G40L12 (Fig. 4a), and two columns with strong upward motion appear in G40L01 (Fig. 4b). The maximum in vertical motion is larger in G40L12 (34×10^{-3} hPa s^{-1}) than in G40L01 (23×10^{-3} hPa s^{-1}), and the maximum value appears near the center in G40L12 and in the upward motion column to the east of the center in G40L01.

Conditional instability in a deep layer existed over the central storm area at the initial time, with θ_e near 350°K at the surface and 342°K at 300 hPa. Also, the atmosphere was conditionally unstable below 700 hPa and stable above 700 hPa beyond 200-300 km from the center. Above cited conditions outside the storm area are maintained in both G40L12 (Fig. 4c) and G40L01 (Fig. 4d) 24 h forecasts. The two forecasts are dissimilar over the storm area. The vertical gradients of θ_e are very weak in the G40L01 central storm area

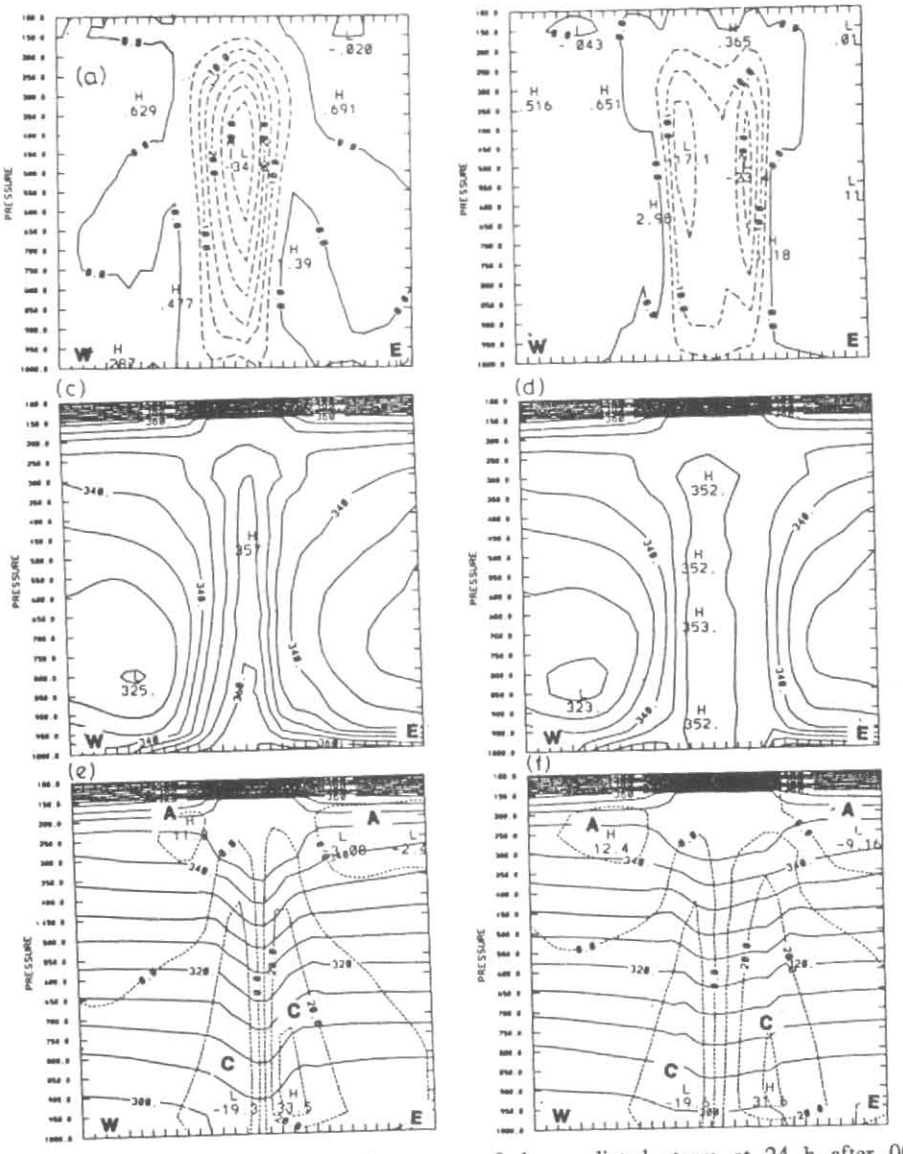

Figs. 4(a-f). West to east cross sections through the center of the predicted storm at 24 h after 0000 UTC 17 August 1991. Vertical motion (10^{-3} hPa s^{-1}): (a) G40L12 and (b) G40L01; equivalent potential temperature (K): (c) G40L12 and (d) G40L01; potential temperature (°K) (solid lines) and tangential wind (ms^{-1}) (dashed lines): (e) G40L12 and (f) G40L01. Cyclonic and anticyclonic winds are denoted by C and A respectively. Ticks on abscissa are at one grid distance interval (*i.e.*, 40 km). See Table 1 for a list of experiments

upto 300 hPa. On the other hand, strong conditionally unstable conditions prevail over the G40L12 central storm area with θ_e greater than 360°K near the surface and below 350°K at 200 hPa. It should be noted that θ_e has increased in the middle and upper troposphere, indicating that an upward flux of moisture and heat has occurred over the central storm area in both forecasts.

The central warm core extends from the surface to above 200 hPa in G40L12 (Fig. 4e). The potential temperatures in G40L01 below 700 hPa are only slightly warmer in the central storm area than in the region outside the storm area (Fig. 4f). Above 700 hPa, the warm core structure is less pronounced in G40L01 than in G40L12. The gradients in tangential velocity are stronger near the center in G40L12 (Fig. 4e) than in G40L01 (Fig. 4f). The maximum tangential velocity occurs at a greater distance to the east of the center in G40L01 than in G40L12.

Surface wind analysis using aircraft reconnaissance data in hurricane Bob has been performed at the Hurricane Research Division, Miami by Samuel H. Houston (personal communication). The strongest winds were located to the east of the center, with maximum value exceeding 30 ms^{-1} (40 ms^{-1}) occurring at about 100 km on 0000 (0600) UTC 18 August. Thus, the

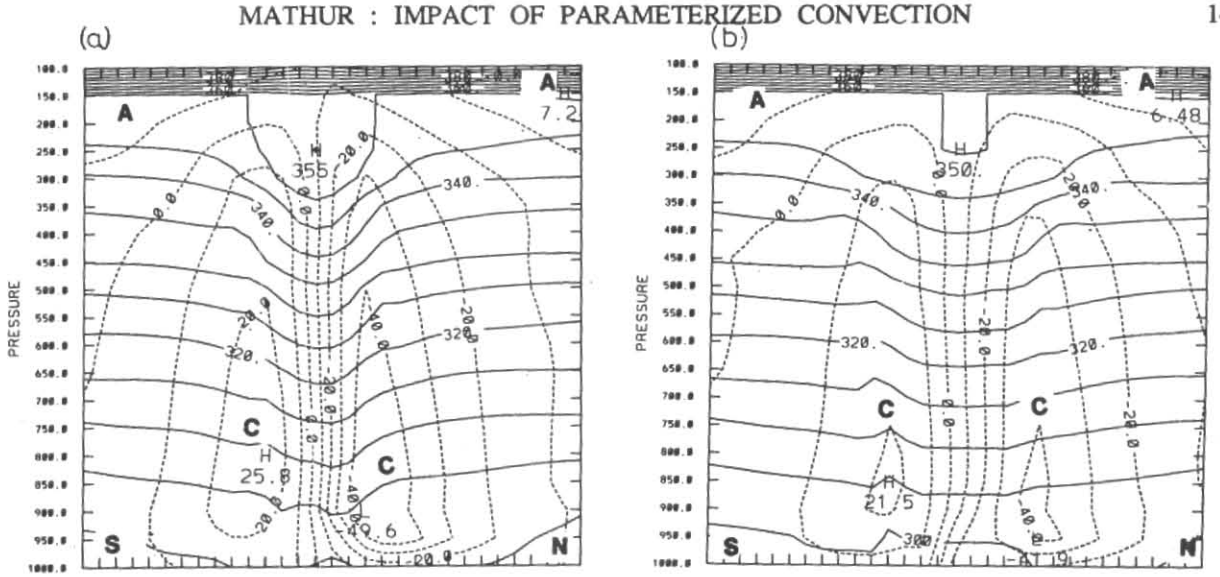

Figs. 5(a-b). South to north cross sections through the center of the predicted storm at 24 h after 1200 UTC 23 August 1992. Potential temperature (°K) (solid lines) and tangential wind (ms^{-1}) (dashed lines): (a) A40L12 and (b) A40L01. Cyclonic and anticyclonic winds are denoted by C and A respectively. Ticks on abscissa are at one grid distance interval (*i.e.*, 40 km). See Table 1 for a list of experiments

distance of the maximum wind from the center is better simulated in G40L12 (100 km) than in G40L01 (200 km).

(3) *Additional results*

Numerical forecasts from other storm cases have also shown that the predicted storm structure depends on the interval at which the condensational heating is evaluated. As an example, the north to south cross sections for the potential temperature and tangential wind at 24 h through the center of the storm for two forecasts from the initial time 1200 UTC 23 August 1992 (a hurricane Andrew case in the Atlantic Ocean) are shown in Fig. 5. The parameterized convection and the resolvable scale heating are evaluated at twelve time step intervals in the first experiment (A40L12) and at each time step in the second experiment (A40L01).

The low level maximum wind in both experiments is located to the north of the center, but its magnitude is greater in A40L12 than in A40L01 (Fig. 5). Strong winds, 40 ms^{-1} to the north and 20 ms^{-1} to the south of the center, extend upward more in A40L12 than in A40L01. The central warm core extends from the surface to 200 hPa in A40L12. The potential temperatures up to 700 hPa in A40L01 are only slightly warmer in the central storm area than in the outer storm area. The warm core structure above 700 hPa is weaker in A40L01 than in A40L12.

(b) *Use of a higher horizontal resolution (grid spacing of 20 km)*

It is shown below that considerably larger differences develop between the two fine mesh forecasts (G20L12 and G20L01) by 12 h, compared to those by 24 h in the two coarse mesh forecasts (G40L12 and G40L01). The predicted fields including the condensational heating rates were saved in G20L12 and G20L01 at one hour intervals, to resolve better the differences in the two fine mesh integrations.

(1) *Vertical motion*

The distribution of 700 hPa vertical velocity ω (units 10^{-3} hPa s^{-1}) at 2, 6 and 12 h in G20L12 and G20L01 is shown in Fig. 6. An inner band A and an outer band B develop by 2 h in both G20L12 (Fig. 6a) and G20L01 (Fig. 6d) and the maximum vertical motion is greater in the later experiment. The outer band is weak in G20L12 except to the southeast of the center, while this band is pronounced in G20L01 and extends from the south to the east and then to the north of the center. The two bands in G20L01 are separated by a semi-circular area with weak upward motion. Weak upward motion occurs in both runs to the west of the center at the above hour.

Both bands become somewhat stronger by 6 h in G20L12 and the maximum in both bands has moved in a counter-clockwise direction (Fig. 6b). Upward vertical motion has also increased in both G20L01 bands (Fig. 6e). Band A at this hour is located to the northwest of the center in both experiments; but as at

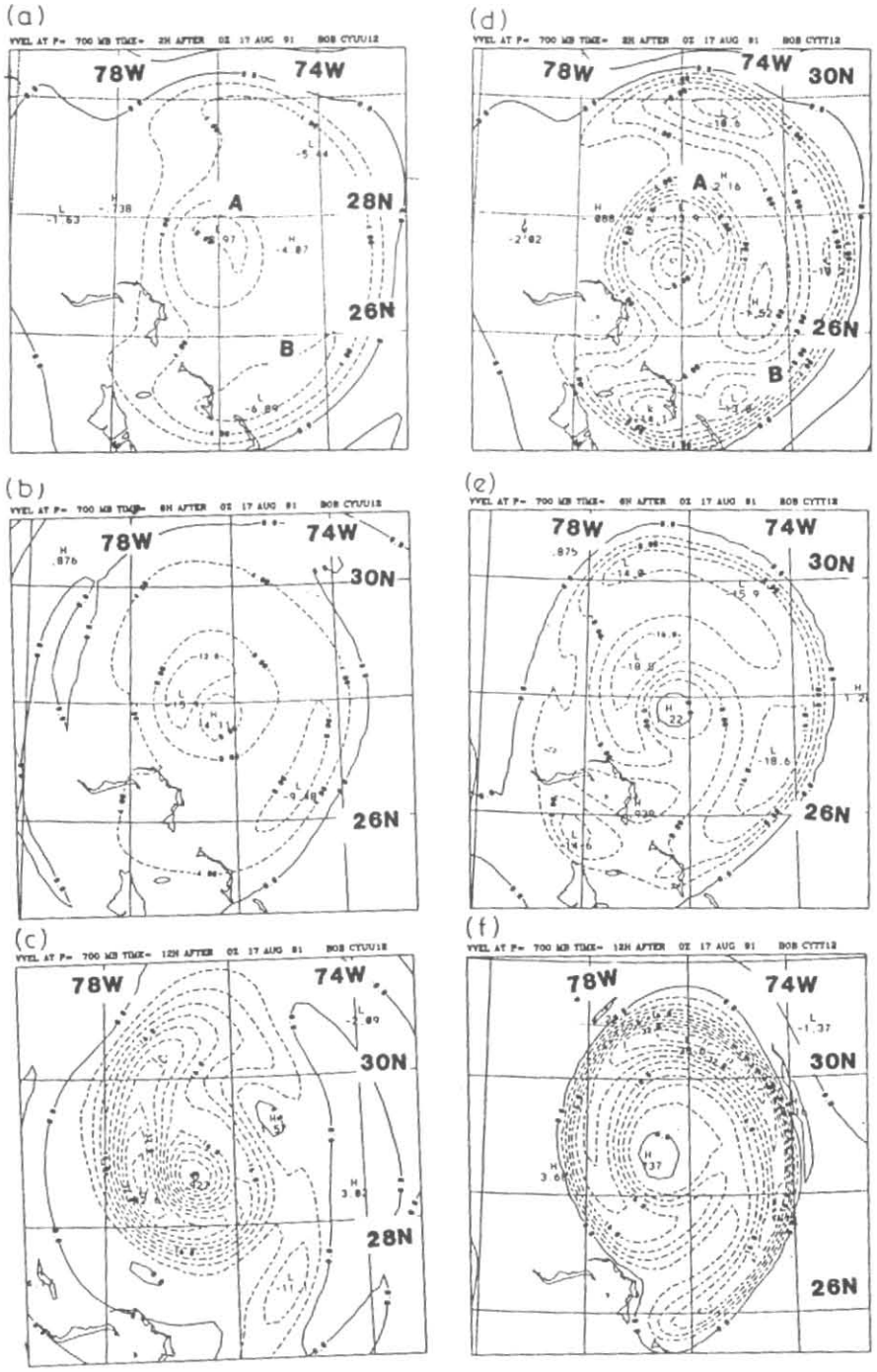

Figs. 6(a-f). Forecast 700 hPa vertical *p*-velocity over the storm area in G20L12 at (a) 2h, (b) 6 h, and (c) 12 h; in G20L01 at (d) 2 h, (e) 6 h, and (f) 12 h. Contour interval is 2×10^{-3} hPa s^{-1} in (a) and (d) and 4×10^{-3} hPa s^{-1} in (b), (c), (e) and (f). The initial time for the forecasts is 0000 UTC 17 August 1991. See Table 1 for a list of experiments

2 h, band B extends over a larger area in G20L01. The vertical motion in areas to the north and east of the center between the two bands has increased considerably in G20L01. An examination of hourly data shows that during the next 6 hours, band A weakens and band B intensifies in G20L01 (Fig. 6f). while band B remains weak and band A intensifies in G20L12 (Fig. 6c). The maximum vertical motion in the G20L01 band B occurs at distance of 300 km to the north of the center. Band A in G20L12 extends from the south to the west and then far to the north of the center, with the maximum vertical motion at 100 km to the west of the center.

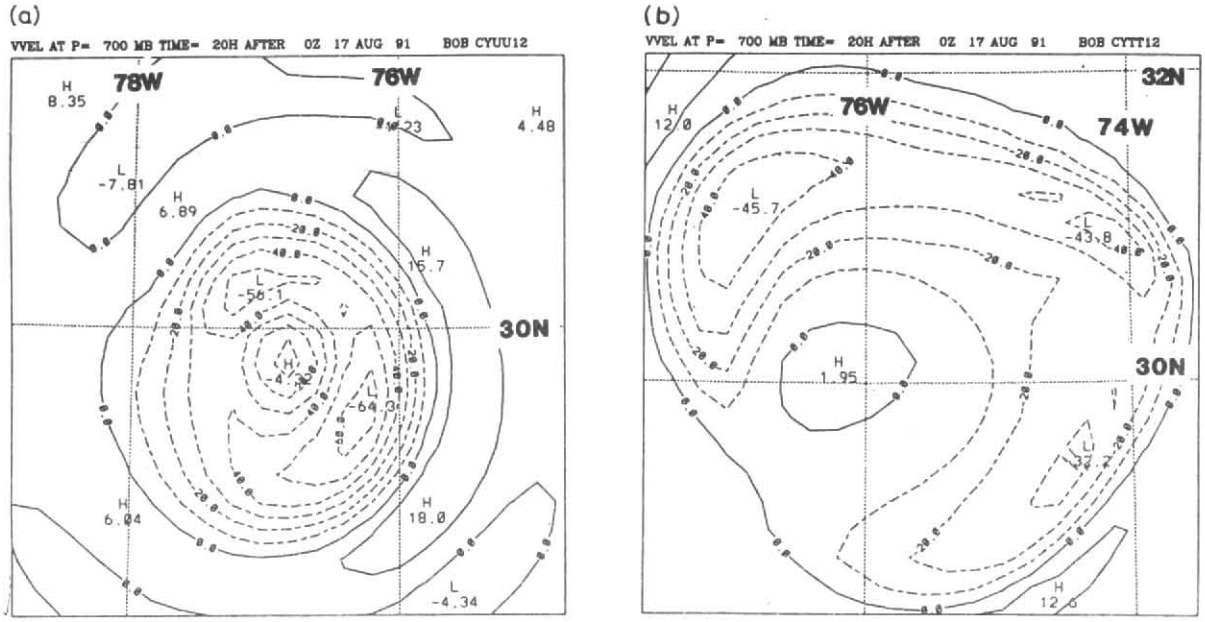

Figs. 7(a-b). Forecast 700 hPa vertical p-velocity in the storm area at 20 h in (a) G20L12, and (b) G20L01. Contour interval is 10×10^{-3} hPa s^{-1}. The initial time for the forecasts is 0000 UTC 17 August 1991. See Table 1 for a list of experiments

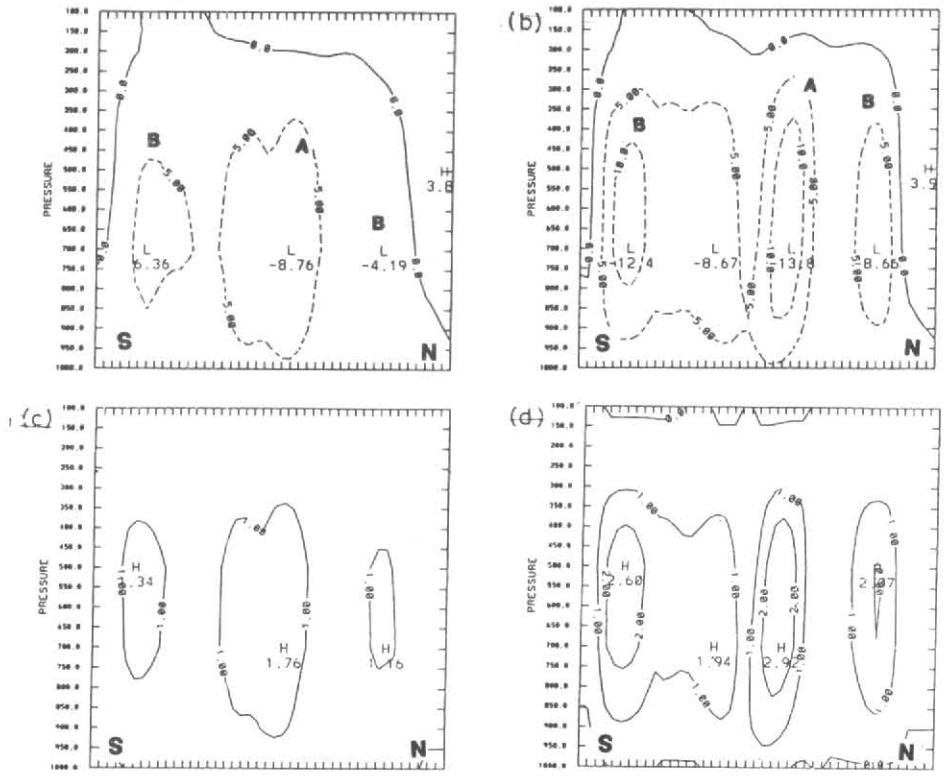

Figs. 8(a-d). South to north cross sections through the center of the predicted storm at 2 h after 0000 UTC 17 August 1991. Vertical motion (10^{-3} hPa s^{-1}) in (a) G20L12 and (b) G20L01. Total condensational heating rate (^{o}K h^{-1}) in (c) G20L12 and (d) G20L01. Ticks on abscissa are at one grid distance interval (*i.e.*, 20 km). See Table 1 for a list of experiments

Vertical motion structure similar to that expected in the eye-wall of a storm first appears at 20 h in G20L12 (Fig. 7a). In place of downward motion at the center, a feature typically observed in a storm, very weak upward motion is simulated. Outside the innermost central area and within 100 km from the center, strong upward motion occurs. A ring of downward motion surrounds the above cited area of upward motion, and a few weak bands with upward motion appear farther from the center. The above

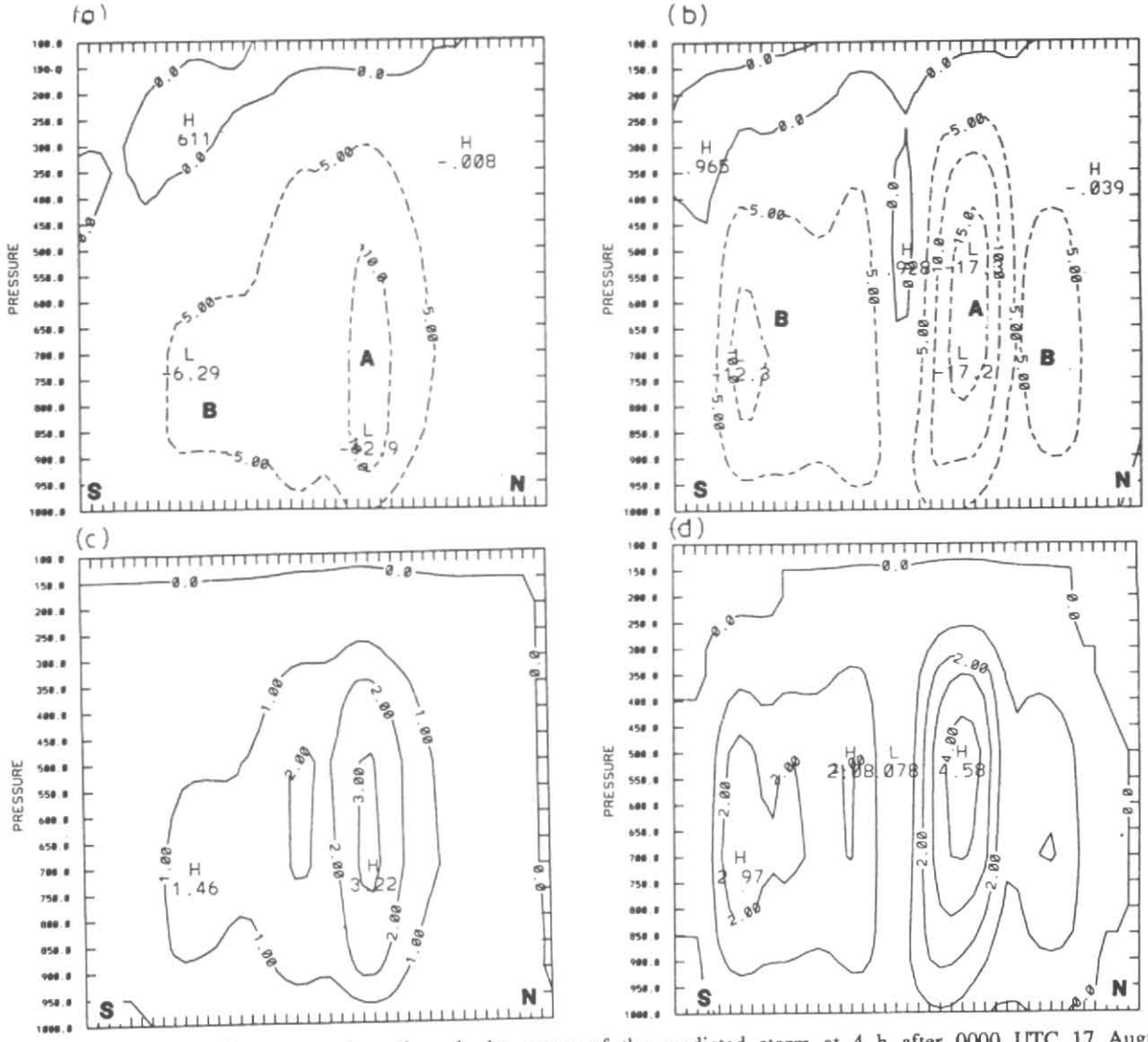

Figs. 9(a-d). South to north cross sections through the center of the predicted storm at 4 h after 0000 UTC 17 August 1991. Vertical motion (10^{-3} hPa s^{-1}) in (a) G20L12 and (b) G20L01. Total condensational heating rate (^{o}K h^{-1}) in (c) G20L12 and (d) G20L01. Ticks on abscissa are at one grid distance interval (*i.e.*, 20 km). See Table 1 for a list of experiments

structure is nearly maintained until the storm reaches the region of upper tropospheric westerlies after 36 h. The structure in G20L01 (Fig. 7b) is very different from that in G20L12. Downward motion occurs over a large central area (about 100 km in diameter), and strong upward motion occurs at a large distance from the center.

(2) *Condensational heating*

South to north cross sections of vertical motion and the total condensational heating at 2 h through the storm center in G20L12 and G20L01 are shown in Fig. 8. Since band B extends from the south to the east and then to the north of the center, this band appears to the north as well as to the south of the center in (Figs 8a & b). The condensational heating (Figs 8c-d) is maximum in the region of the bands. The vertical motion and the condensational heating are stronger in G20L01 than in G20L12. Also, the heating rates exceeding $1^{o}K$ h^{-1} extends into higher levels in G20L01 than in G20L12. The maximum upward motion is larger in G20L01 (Fig. 9b) than in G20L12 (Fig. 9a) at 4 h, and the maximum condensational heating in band A is larger and is located at a higher level in G20L01 (Fig. 9d) than in G20L12 (Fig. 9c). Both the resolvable and convective scale heating rates were greater in G20L01 than in G20L12 during the first four hours.

Horizontal structure of the vertical velocity at 10 h was similar to that at 12 h (Fig. 6) in both integrations. Strong vertical motion occurs from the north to the west and then to the south of the center in G20L12

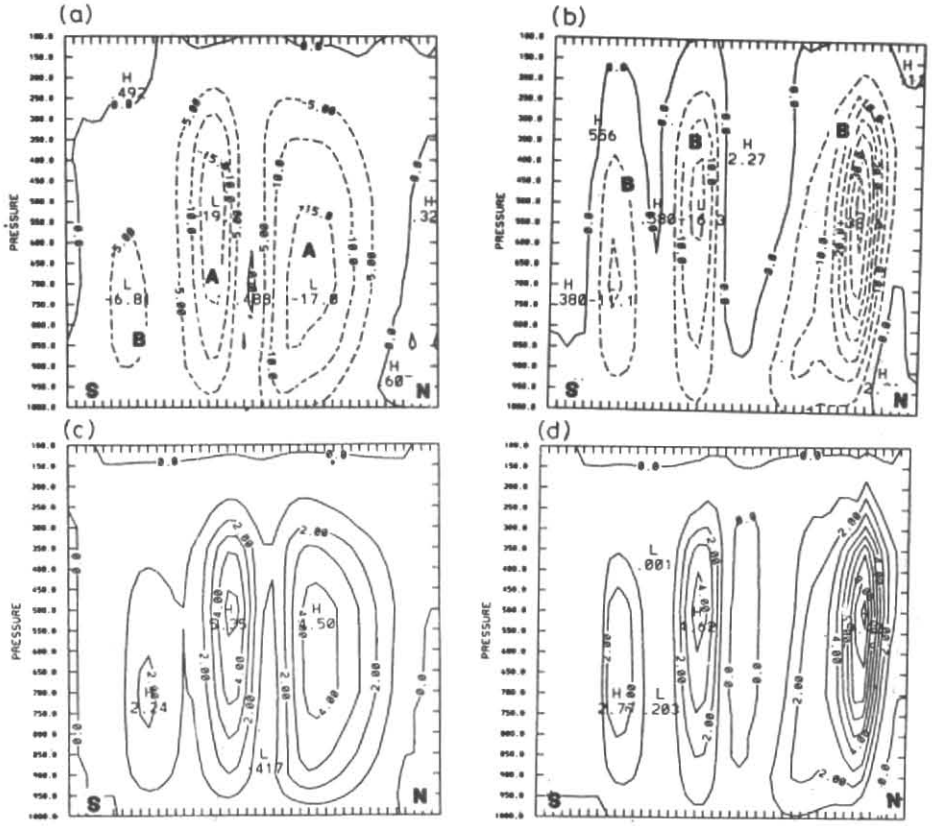

Figs.10(a-d). South to north cross sections through the center of the predicted storm at 10 h after 0000 UTC 17 August 1991. Vertical motion (10^{-3} hPa s^{-1}) in (a) G20L12 and (b) G20L01. Total condensational heating rate (^{o}K h^{-1}) in (c) G20L12 and (d) G20L01. Ticks on abscissa are at one grid distance interval (i.e., 20 km). See Table 1 for a list of experiments

band A. Therefore, the two maximums in vertical motion, one to the north and the other to the south of the center in (Fig. 10a), are in band A. Band B in G20L01 extended from far to the south (200-300 km), to the east, to the north, to the west and then just to the south of the center. All three columns with large upward motion in (Fig. 10b) are located in band B. Strong condensational release of latent heat occurs in areas with significant upward motion in both experiments. Both the vertical motion (Fig. 10a) and the condensational heating (Fig. 10c) are largest in G20L12 just to the south of the center. The heating in G20L01 is very large (9^{o}K h^{-1}) in the northern portion of band B (Fig. 10d) where the upward motion is strongest (Fig. 10b).

(*i*) *Conditional instability* — The distribution of $\partial\theta_e$ / ∂p at a low tropospheric layer (900 hPa) at 6 h in G40L12 (Fig. 3a) and G20L12 (Fig. 11a) is similar except near the center. At about 200-400 km from the center, high values (> 80×10^{-3} ^{o}K hPa^{-1}) occur to the northwest and northeast, and low values occur to the south and north, of the center in both experiments. Strong gradients of $\partial\theta_e$ / ∂p near the center develop in G20L12 but not in G40L12 at 6h. Recall that strong gradients appear in G40L12 at later hours (section 3a). The structure of $\partial\theta_e$ / ∂p at 900 hPa in G40L01 (Fig. 3b) and G20L01 (Fig. 11b) is very similar; storm's central area has become stable in both G40L01 and G20L01.

(3) *Additional differences*

Storm motion and intensity were somewhat better predicted in G20L12 than in G20L01 (Table 2). The central mean sea level pressure at 12 h was lower in G20L12 (996 hPa) than in G20L01 (1001) hPa. Maximum pressure gradient value was greater in G20L01 than in G20L12; it was located at about 250 km in G20L01 to the northeast, and at about 100 km in G20L12 to the southeast, of the center. The maximum wind was stronger in G20L01 (33 ms^{-1}) than in G20L12 (28 ms^{-1}), and it was located at a greater distance in G20L01 (200 km) than in G20L12 (100 km). Maximum in rainfall in G20L12 was located at 100 km to the west of the center, while it was located in G20L01 at about 250 km to the north of the center.

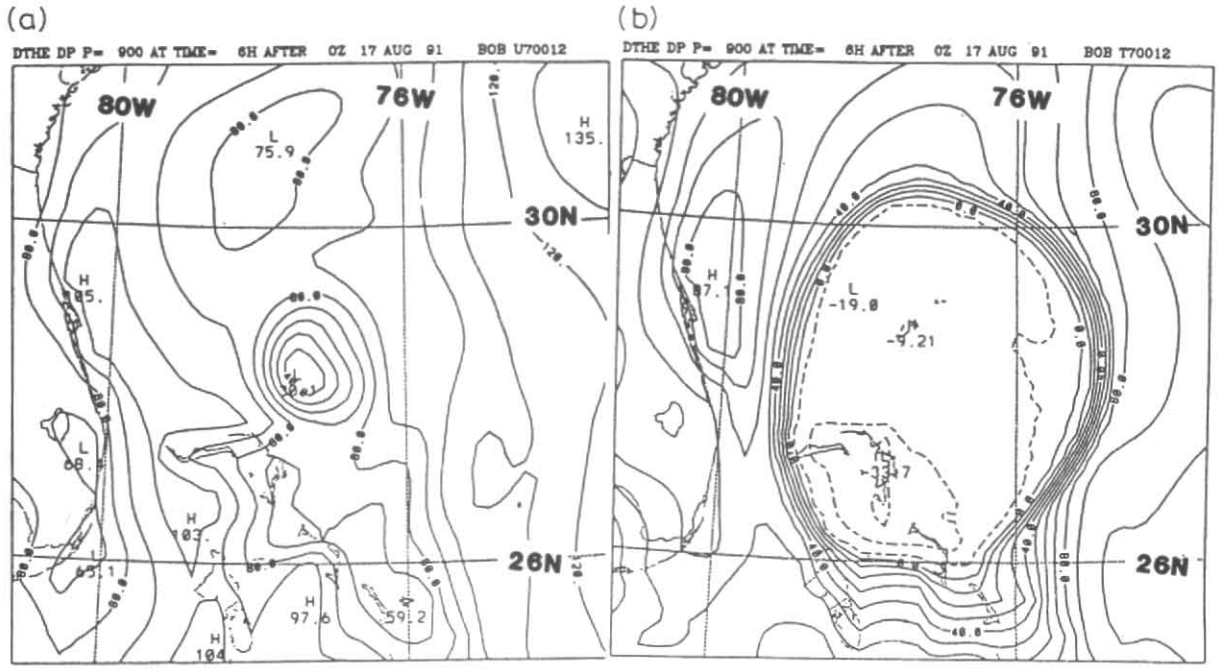

Figs.11(a-b). Distribution of $\partial\theta_e/\partial p$ (10^{-3}°K hPa^{-1} at 6h in (a) experiment G20L12 and (b) experiment G20L01. The initial time for the forecasts is 0000 UTC 17 August 1991. See Table 1 for a list of experiments

4. Fully explicit heating

Some authors (*e.g.*, Ooyama 1982, Arakawa and Chen 1986, Molinari and Dudec 1992) have argued that it may not be always appropriate to use parameterized convection in models that can simulate mesoscale circulations. It has been suggested that the spectral gap between convective scale and mesoscale does not exist, and employment of a parameterization scheme to include effects of convection in mesoscale models may be ambiguous. Additionally, previous studies have shown that a hurricane-like structure can be simulated without the parameterized convection (see the last paragraph of this section); the results from experiments one with and the other without the parameterized convection would illuminate relative importance of the two condensation processes in the development of the predicted storm. The QLM was integrated without the parameterized convective heating and with resolvable scale (explicit) condensational heating evaluated at each time step (experiment G20NC1). A comparison of G20L12, G20L01 and G20NC1 is now presented.

(a) *Banded structure*

Vertical motion structure at 6 h in G20NC1 (Fig. 12a) resembles that in G20L12 (Fig. 6b) in some respects and that in G20L01 (Fig. 6e) in some other aspects. Maximum upward motion in band B is weaker than in band A in both G20L12 and G20NC1, while it has nearly the same magnitude in both bands of G20L01. Band B is well marked in both G20NC1 and G20L12 only to the southeast of the center. The maximum upward motion in band A is higher in G20L01 and G20NC1 than in G20L12. Notice also that band A is located in G20NC1 to the west, and in G20L12 and G20L01 to the northwest, of the center. Downward or weak upward motion in storm central area appears in all three experiments. A narrow area of weak vertical motion between the two bands is produced at about 150 km to the south of the center in both G20L01 and G20NC1.

As in G20L12, band B remains weak and band A intensifies in G20NC1 by 12 h (Fig. 12b). However, band B is weaker and band A is much stronger in G20NC1 than in G20L012 (Fig. 6c). On the other hand, band B intensifies and band A weakens by 12 h in G20L01 (Fig. 6f). It should be also noted that band A is much narrower, especially to the north of the storm center, in G20NC1 than in G20L12. The maximum vertical motion in band A has increased in magnitude from -19×10^{-3} hPa s^{-1} at 6 h to -111×10^{-3} hPa s^{-1} by 12 h in G20NC1, while it increased from -15×10^{-3} hPa s^{-1} to -42×10^{-3} hPa s^{-1} in G20L12 during the same period.

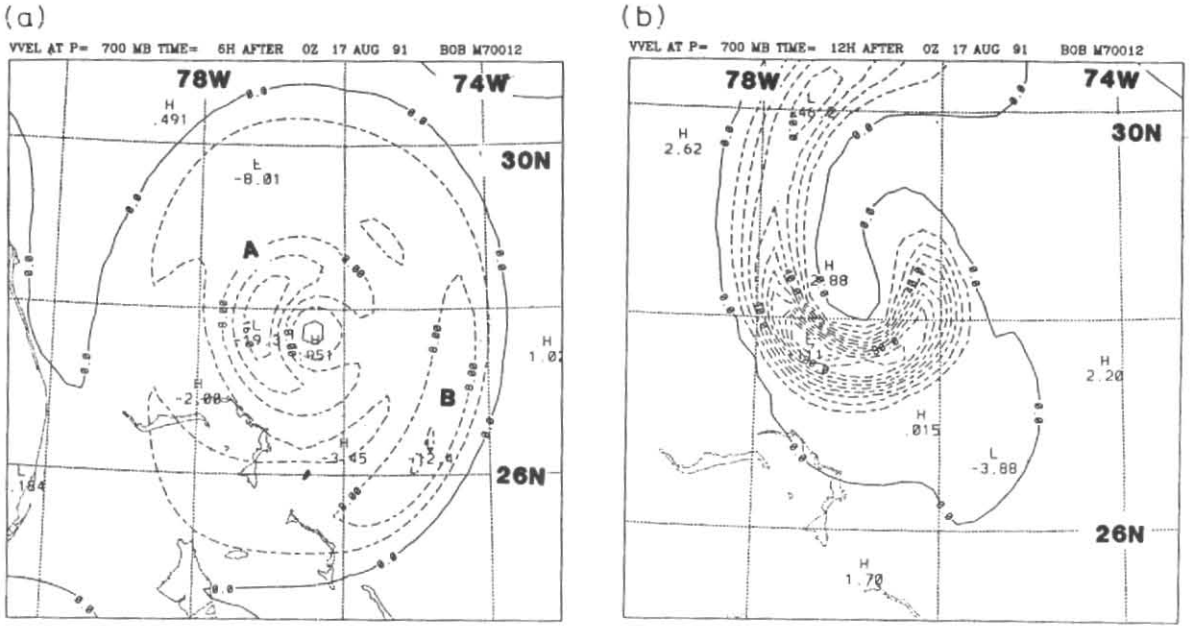

Figs.12(a-b). Forecast 700 hPa vertical p-velocity (10^{-3} hPa s^{-1}) in G20NC1 over the storm area at (a) 6 h, and (b) 12 h. The initial time for the forecasts is 0000 UTC 17 August 1991. See table 1 for a list of experiments

Forecast central pressure at 12 h was closer to the observed (996 hPa) in G20L12 (996 hPa) than in G20L01 (1001 hPa) or G20NC1 (992 hPa). The storm structure and intensity were better after 24 h in G20NC1 and G20L12 than in G20L01 (not shown).

(b) *Vertical distribution of heating*

Vertical cross sections of resolvable scale heating ($^{o}K\ h^{-1}$) in G20NC1 at 2 h, 4h, and 10 h are shown in Fig. 13. The structure of total heating in G20L12 (Fig. 8c) and G20NC1 (Fig. 13a) is similar at 2 h. On the other hand, the total heating in the middle troposphere at 2 h is greater in G20L01 (Fig. 8d) than in G20L12 or G20NC1. Structure and intensity of total heating at 4 h is similar in G20L12 (Fig. 9c) and G20NC1 (Fig. 13b). The total heating in the middle troposphere in both A and B band areas is greater in G20L01 (Fig. 9d) than in G20L12 or G20NC1.

Two columns with significant heating (marked C and D in Fig 13c), one far to the south and the other near the center, have nearly the same location at 10 h in G20L12 (Fig. 10c), G20L01 (Fig. 10d) and G20NC1. A third column with significant heating (marked E in Fig. 13c) has the same location in G20L01 and G20NC1, but it is located closer to the center in G20L12. The maximum total heating in C is largest ($2.7^{o}K\ h^{-1}$) in G20L01, and it is somewhat lower in G20NC1 and G20L12. Total heating in D is much greater in G20NC1 than in G20L12 or G20L01; the maximum value is about $13^{o}K\ h^{-1}$ in G20NC1, and greater (less) than $5^{o}K\ h^{-1}$ in G20L12 (G20L01). The heating rates in E are greater in G20L01 than in G20NC1; the maximum value is about $4^{o}K\ h^{-1}$ in G20NC1 and greater than $9^{o}K\ h^{-1}$ in G20L01. As noted above, E is located closer to the center in G20L12, and the maximum heating rate is about $4^{o}K\ h^{-1}$.

Development of hurricanes, incorporating only the explicit condensational release of latent heat, has been studied previously (Yamasaki 1977 and Rosenthal 1978). Yamasaki employed a nonhydrostatic, and Rosenthal a hydrostatic, axi-symmetric set of equations. Microphysical processes were included in both studies while these are not included in the QLM. However, Rosenthal (1978) suggests that the inclusion of these processes is not critical for simulating the development of a hurricane. On the other hand, Zhang *et al.* 1988, and Hong and Lee 1994 have shown that the inclusion of microphysical processes leads to a better prediction of mesoscale rainfall in convective extratropical storms. These authors also found that excessive rainfall at isolated grid points develops in their model when all or part of the microphysics (like evaporation of rain and cloud water) is excluded; this kind of instability, however, did not develop in the QLM run cited above in which only the large scale latent heating

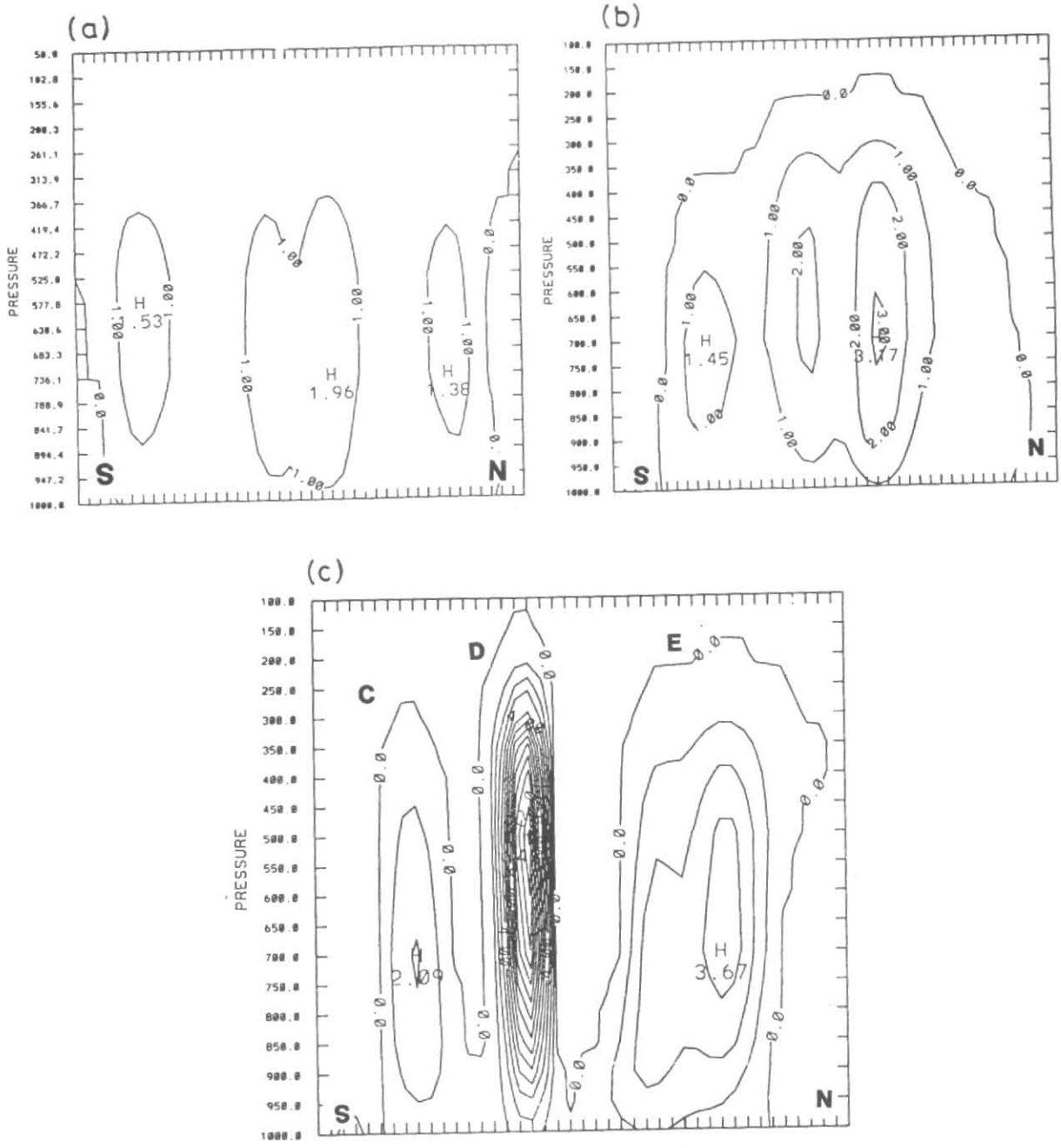

Figs.13(a-c). South to north cross sections of condensational heating ($^{o}K\ h^{-1}$) through the center of the predicted storm in G20NC1 at (a) 2 h, (b) 4 h, and (c) 10 h. The initial time for the forecasts is 0000 UTC 17 August 1991. Ticks on abscissa are at one grid distance interval (*i.e.*, 20 km). See Table 1 for a list of experiments

was included. It should be also noted that precipitation first develops in Rosenthal (1978) after 9 h, and Yamasaki (1977) introduced buoyancy perturbations to initiate convection at different radii. In Jones (1986) study a three dimensional hurricane model that utilized (idealized) initial conditions and physical processes similar to those employed in Rosenthal (1978) model was integrated, realistic banded structure developed after 280 h. Our initial conditions are based on observations (section 2), and bands with significant latent heating develop within two hours.

5. Ancillary experiment results

A series of supplementary experiments were conducted to further clarify the dependence of model storm structure on horizontal resolution and on frequency at which the parameterized convective heating and the resolvable scale condensation are evaluated. The fine mesh version of the QLM (section 2) is utilized in the ancillary experiments, and the results from these experiments are compared with those described in sections 3-4.

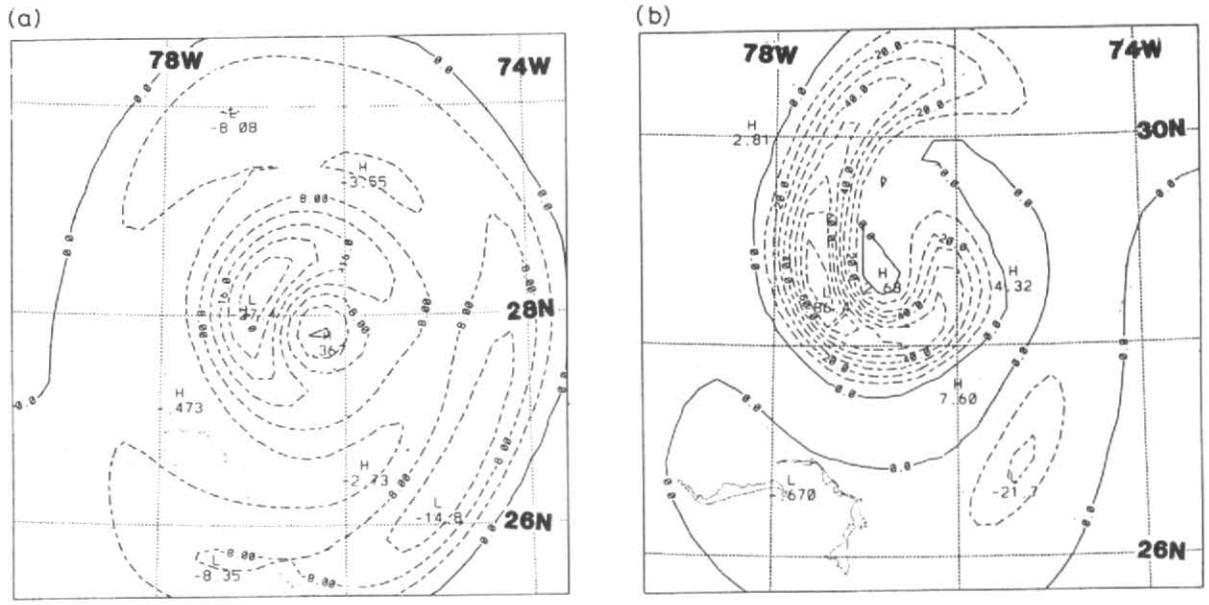

Figs.14(a-b). Forecast 700 hPa vertical p-velocity over the storm area in G20NC12R1 at (a) 6 h, and (b) 12 h. Contour interval is 4×10^{-3} hPa s^{-1} in (a) and 10×10^{-3} hPa s^{-1} in (b). The initial time for the forecasts is 0000 UTC 17 August 1991. See Table 1 for a list of experiments

(a) *Use of same condensation interval in both fine and coarse mesh experiments*

Condensational processes are evaluated at twelve time step intervals in the original QLM. Thus, the interval for evaluating condensation processes was not the same in G40L12 (600 s) and G20L12 (480 s). For elucidating further the impact of horizontal resolution and interval for evaluating condensation on storm structure, the condensation processes were evaluated at 600 s (fifteen time steps) intervals in G20L16 (Table 1). The impact of increasing the interval for evaluating condensation from 480 s to 600 s was not large; the vertical motion composition at 6 and 12 h in G20L15 (not shown) and G20L12 were similar. Also, the differences between G20L12 and G40L12 were similar to those between G20L15 and G40L12. The structural dissimilarities between G20L12 and G20L01 were similar to those between G20L15 and G20L01.

(b) *Use of different intervals for two condensation processes*

For elucidating further the impact of changing the interval for calculating parameterized convection on storm structure, the resolvable scale condensation was evaluated at every time step and the parameterized convection at intervals of twelve time steps in the experiment G20C12R1. A comparison of Figs. 14 a-b, 6b-c, and 6e-f indicates that the evolution of vertical motion in G20C12R1 is much closer to G20L12 than G20L01. Notice that the maximum vertical motion at 12 h is located at about 100 km to the west of the center in both G20L12 and G20C12R1 while the maximum in vertical motion occurs at a larger distance (300 km) to the north of the center in G20L01. The maximum vertical motion is, however, much greater at both 6 h and 12 h in G20C12R1 than in G20L12.

The convective heating is invoked at intervals of twelve time steps in both G20L12 and G20C12R1, and the resolvable scale condensation is evaluated at an interval of twelve time steps in G20L12 and at each time step in G20C12R1. A comparison of vertical motion fields discussed above in G20L12 and G20C12R1 portend that changing the interval for evaluating resolvable scale condensation from twelve time steps to one time step enhances the storm development.

Resolvable scale condensation is evaluated at each time step in G20L01 and G20C12R1. The only difference between the two experiments is that the parameterized convection is invoked at each step in G20L01 and at intervals of twelve time steps in G20C12R1. This difference causes considerable dissimilarities in the storm structure predicted in two cases. It was noted in section 3b that evaluation of convective heating at each time step (in G20L01) causes stabilization of vertical columns in the central storm area; and this transformation induces the shifting of the area with large condensational heating, maximum

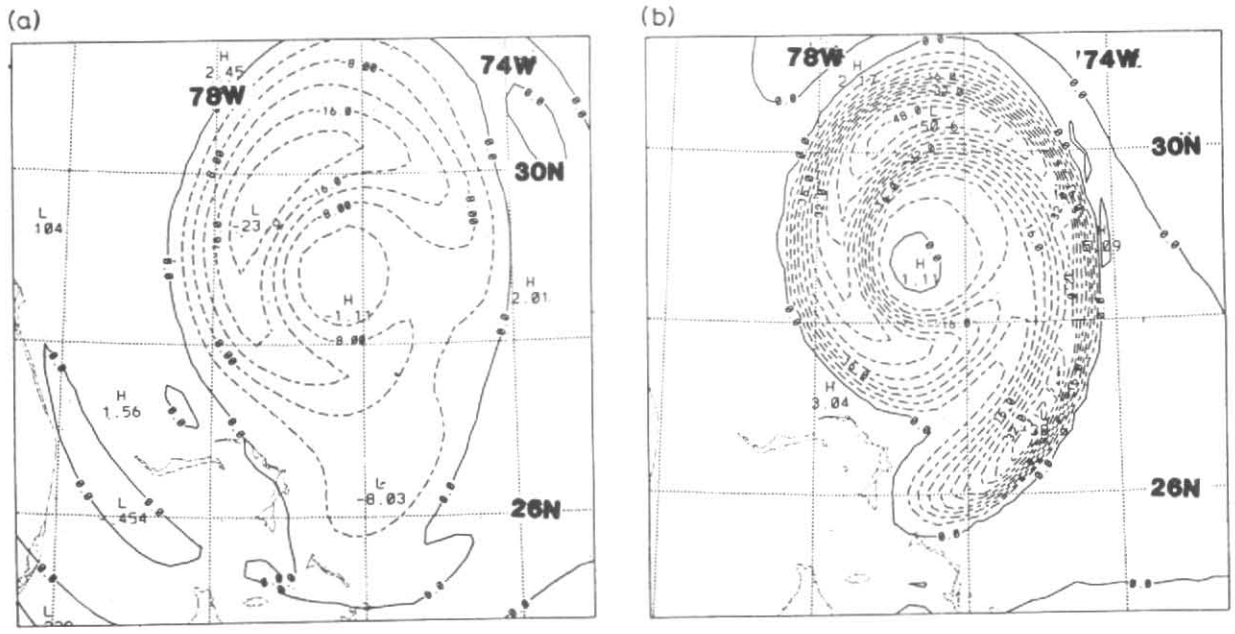

Figs.15(a-b). Forecast 700 hPa vertical *p*-velocity over the storm area at 12 h after 0000 UTC 17 August 1991 in (a) G20L1L12, and (b) G20L12L1. Contour interval is 4×10^{-3} hpa s^{-1}. See Table 1 for a list of experiments

vertical motion and strong winds to a considerable distance from the center. Consequently, a large storm develops in G20L01. On the other hand, when parameterized convection (G20C12R1) is evaluated at intervals of twelve time steps, maximum vertical motion develops close to the center because the stabilization of the central area does not occur; and a storm of size smaller than G20L01 develops.

The interval for evaluating resolvable scale condensation is the same (one time step) in both G20NC1 and G20C12R1. The difference between the two experiments is that the parameterized convection is excluded from G20NC1 and it is invoked at intervals of twelve time steps in G20C12R1. The maximum vertical motion in G20C12R1 at 6 h is greater and at 12 h lower than in G20NC1 (compare Figs. 14 a-b and 12a-b). Although the storm circulation develops more rapidly initially in G20C12R1 than in G20NC1, the inclusion of parameterized convection abates the storm development after first few hours. The above cited results show that the impact on storm structure of changing the interval for evaluating either condensational heating is large.

(c) *Model spin up*

Diabatic effects are often not simulated well initially in a numerical model because of poor analysis particularly of moisture and divergence fields, or due to imbalances in the initial fields. Because of the above cited deficiencies, a spin up often occurs during the first few hours of integration, and thereafter the model generally approaches a dynamically and physically balanced state. It may be argues that substantial differences that develop between G20L12 and G20L01 during the first six hours are mainly due to the spin up. Two additional 6-hour forecasts were made to diagnose further the impact of changing the interval for computing condensational physics on the QLM predictions. The 6 h forecast fields from G20L01 (G20L12) are used as the initial conditions in the experiment G20L1L12 (G20L12L1). Both parameterized convection and resolvable scale condensation are evaluated at intervals of twelve time steps in G20L1L12 and at each time step in G20L12L1. The maximum vertical motion at 12 h is located to the north of the center in G20L01 (Fig. 6f) and G20L12L1 (Fig. 15b), and to the west to northwest of the center in G20L12 (Fig. 6c) and G20L1L12 (Fig. 15a). Also the vertical motion is much stronger to the east of the center in G20L01 and G20L12L1 than in G20L12 and G20L1L12. The vertical motion structure at 12 hours after 0000 UTC 17 August in G20L1L12 (Fig. 15a) is closer to G20L12 (Fig. 6c) than G20L01 (Fig. 6f); while the vertical motion structure at the above hour in G20L12L1 (Fig. 15b) is closer to G20L01 (Fig. 6f) than G20L12 (Fig. 6c).

A synthesis of the results cited in the above paragraph is now presented. Condensation processes are evaluated at intervals of twelve time steps in

G20L12 and at each time step in G20L01 throughout the integration period (Table 1). A major difference at 6h in G20L12 (Fig. 6b) and G20L01 (Fig. 6e) is that the maximum vertical motion in band A is stronger than in band B in G20L12, but the maximum vertical motion is nearly of the same magnitude in both bands of G20L01. Another significant difference is that band B extends over a larger area in G20L01 than in G20L12. We showed in section 3b that during the 6-12 h period, the inner band A intensifies and the outer band B remains weak in G20L12 (Fig. 6c); on the other hand, band B intensifies and band A weakens in G20L01 (Fig. 6f). When the interval for evaluating condensation is changed at 6h from 12 time steps to each time step in G20L12L1 (6 h forecast from G20L12 is used as the initial state), strom structure (Fig. 15b) similar to G20L01 (Fig. 6f) develops; *i.e.*, band B intensifies and band A weakens. When the interval for evaluating condensation is changed at 6 h from each time steps in G20L1L12 (6 h forecast from G20L01 is used as the initial state), storm structure (Fig. 15a) closer to G20L12 (Fig. 6c) than G20L01 develops; *i.e.*, band A intensifies and band B remains weak. The above cited results imply that the storm structure in our experiments largely depends on the interval at which the condensation is evaluated, and the differences in forecast structure with the change in interval for evaluating condensation processes are not due to the initial spin up associated with the imbalances or other deficiencies in the initial state.

(d) *Use of Kuo (1974) parameterization scheme*

Convective parameterization scheme based on Kuo (1965) was used in the experiments described above. In Kuo type scheme, a portion b of the moisture available in a column to produce convective clouds is used to moisten the column, and the remaining part is condensed (induces warming of the column). For a typical tropical sounding, b from Kuo (1965) scheme lies close to 1, which implies that most of the moisture available is utilized for moistening the column. Kuo (1974) used observations presented in Reed and Recker (1991) and estimated that in the regions of low level convergence, only a small fraction of moisture available to produce convective clouds is used to moisten the column. Various procedures have been proposed to specify the parameter b (Anthes 1977, Krishnamurti *et al.* 1980). Anthes expressed b as a function of mean relative humidity:

$$b = [(1 - \langle RH \rangle)/(1 - RH_c)]^n \text{ for } \langle RH \rangle \geq RH_c, \text{ otherwise } b = 1 \quad (1)$$

Here, RH is relative humidity, and $\langle\ \rangle$ denotes the vertically averaged value of the variable over the cloud depth. Use of n between 2 and 3 and RH_c between 0.25 and 0.50 gave the best agreement between observed and diagnosed values (Kup and Anthes 1984). Dr Peter Caplan (personal communication) incorporated the following specification for b in NMC's Medium Range Forecast Model (see NMC Development Division 1988).

$$b = 1 - \langle q \rangle / \langle q_s \rangle \quad (2)$$

Here q is the specific humidity, and the subscript s denotes the saturation value. The value of b from Eqn. (1) may differ considerably from that obtained from Eqn. (2). As an example, in the regions where an atmospheric column is nearly saturated in the lower troposphere and dry in the upper troposphere, b based on specific humidity (Eqn. 2) is likely to be lower and more appropriate than one based on relative humidity (Eqn. 1). We now present results from experiments G20L12B and G20L01B in which Kuo (1974) scheme is utilized, with the definition of b given by Eqn. 2. Both condensation processes are evaluated at intervals of twelve time steps in G20L12B, and at each time step in G20L01B (Table 1).

Storm structure similar to G20L12 developed in G20L12B by 12 h. Band A is much stronger than band B at 12 h in both G20L12 (Fig. 6c) and G20L12B (Fig. 16a). The maximum upward vertical motion exceeding 40×10^{-3} hPa s^{-1} is located at about 100 km to the west of the center at the above hour in both experiments. The vertical motion structure at 20 h is also similar in G20L12 (Fig. 7a) and G20L12B (Fig. 16b); notice that the maximum vertical motion in the band surrounding the center occurs in two areas, one to the east and the other to the north of the center, in both experiments.

The vertical motion structure at 12 h in G20L01B (Fig. 16c) is clearly much closer to G20L01 (Fig. 6f) than G20L12 (Fig. 6c). The structure at 20 h in G20L12 (Fig. 7a) and G20L12B (Fig. 16b) is more circular than in G20L01 (Fig, 7b) or G20L01B (Fig. 16d). The upward motion area is larger in G20L01 and G20L01B than in G20L12 or G20L12B. The 850 hPa maximum wind 49 ms^{-1} (48 ms^{-1}) at 20 h was located at about 80 km (140 km) from the center in G20L12B (G20L01B). Thus, structural differences produced with the change in interval for evaluating two condensation processes using Kuo (1974) type scheme are similar to those obtained using Kuo (1965) scheme.

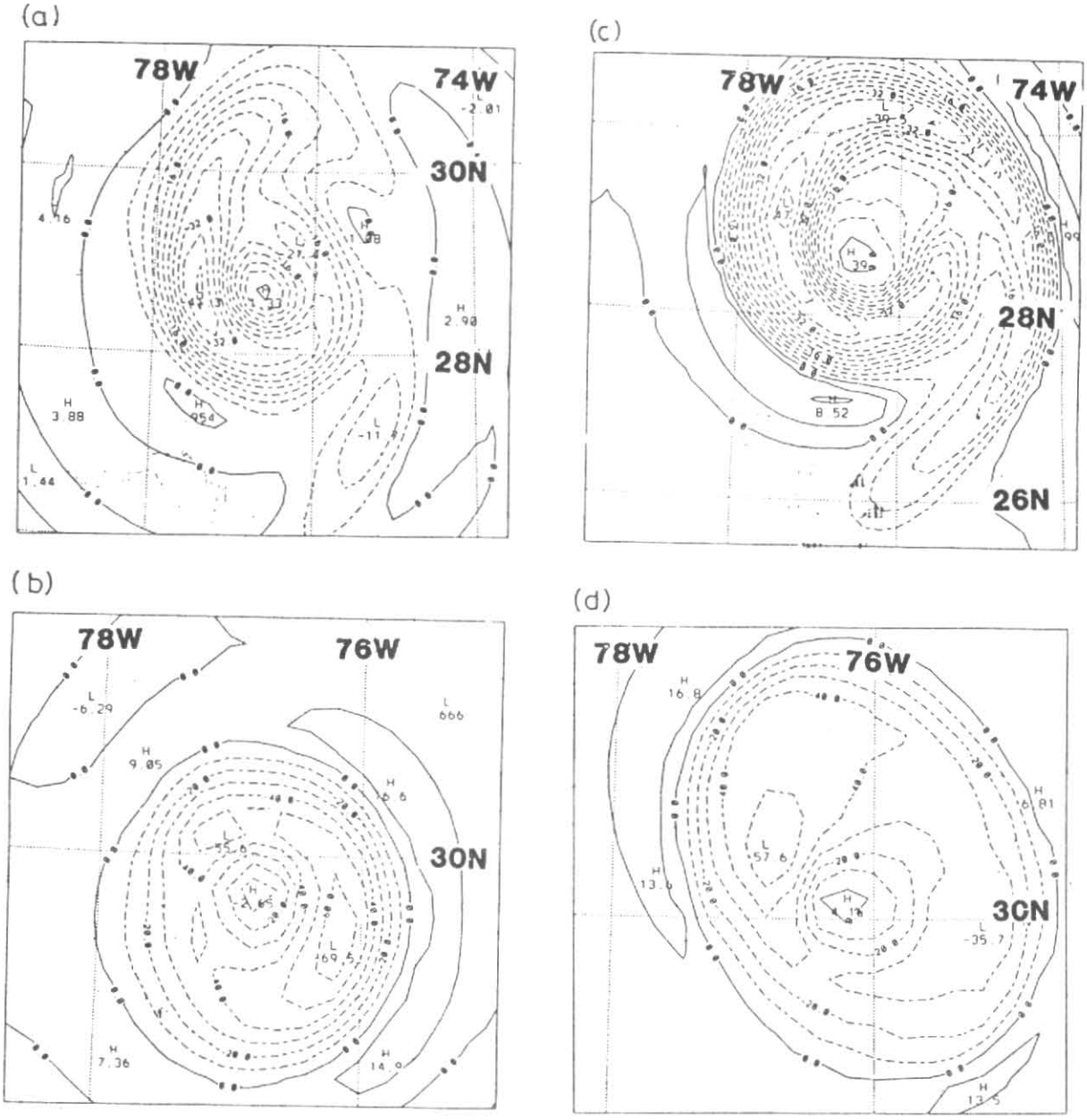

Figs.16(a-d). Forecast 700 hPa vertical p-velocity over the storm area in G20L12B at (a) 12 h, and (b) 20 h; in G20L01B at (c) 12 h, and (d) 20 h. Contour interval is 4×10^{-3} hPa s^{-1} in (a) and (c), and 10×10^{-3} hPa s^{-1} in (b) and (d). The initial time for the forecasts is 0000 UTC 17 August 1991. See Table 1 for a list of experiments

6. Summary and conclusions

Numerical forecasts from NCEP's Quasi-Lagrangian Model were carried out to study the impact on tropical storm structure of varying the horizontal resolution and the interval for invoking parameterized convection and the resolvable scale condensation, and of excluding the parameterized convective heating. A Kuo-type convective parameterization scheme was employed. Resolvable scale condensation was invoked only at grid points where the relative humidity exceeded 100%. A time step of less than a minute was used in our experiments; the time step, resolution and interval used for invoking condensation processes in the experiments are provided in Table 1.

Storm intensity and structure were considerably improved when the horizontal resolution was increased (section 3). A comparison of G20L12 and G20L01, G20L12B and G20L01B, and of G40L12 and G40L01, showed that tropical storm intensity, structure and motion were simulated better in both coarse and fine mesh forecasts, when parameterized convection and resolvable scale condensation were invoked at an

interval of twelve time steps than one time step (see Table 2 and sections 3-5).

A mechanism for the development of the above differences between G20L12 (G40L12) and G20L01 (G40L01) is now presented. At the initial time, conditionally unstable conditions from the surface to 300 hPa prevailed over the storm central area (section 3a). During the first two hours, the total condensation was greater when the parameterized convective release of latent heat in the storm area was computed at each time step (G20L01) than when it was evaluated at intervals of twelve time steps (G20L12) (see Fig. 8). This difference in heating induced larger upward motions in G20L01 than in G20L12. By 4 h, the vertical motion and the condensational heating in the inner storm area became much larger in G20L01 than in G20L12 (Fig. 9). Because of the rapid heating of deep vertical columns in G20L01, the conditional instability in the central storm area decreased and the atmosphere in the low troposphere became convectively stable by 6 h (Fig. 11b). The maximum condensational heating after 6 h occurred in the outer band in G20L01 and in the inner band in G20L12 (Fig. 10). Consequently, large pressure gradients, and strong horizontal winds developed at a greater distance from the center in G20L01 than in G20L12 (section 3b). Note that many circulation differences similar to those between G20L12 and G20L01 also developed between G40L12 and G40L01 (section 3a). Mesoscale structure is simulated better in the fine mesh than in the coarse mesh forecasts. The impacts of a change in interval for evaluating condensation is large on mesoscale features. Therefore, differences are greater in two fine mesh than in two coarse mesh predictions.

Dissimilarities that arise due to a change in the interval for evaluating condensational heating are also explicable on the difference in static stability produced in our experiments. As an example, the static stability after the first few hours in the storm area is greater in G20L01 (parameterized convection is evaluated at each time step) than in G20L12 (parameterized convection is evaluated at intervals of twelve time steps). Rossby's radius of deformation depends on the static stability; and this radius, and therefore the size of the storm, will be greater in G20L01 than in G20L12.

Because parameterized convection tends to stabilize a vertical column, the intensification of the predicted storm over first 12 hours is lower when the convective parameterization is included than when it is excluded (section 5). Vigorous heating takes place in a few deep vertical columns in G20NC1, and the heating rate is very large in a narrow area near the center (marked D in Fig. 13c). The vertical motion was also large in this area. Strongest vertical motion and the maximum in resolvable scale heating occur in the middle troposphere. The above results suggest that the heating on the convective scale in this narrow column is simulated as a resolvable scale release of latent heat. It should be noted that in other studies mentioned in section 4b in which a tropical storm is simulated without a convective parameterization procedure. (Rosenthal 1978), the heating on the convective scale is also simulated as the resolvable scale heating.

A time step of the order of a minute is used in many fine mesh models that use a grid spacing of 20-50 km. Consider a grid point in such a model that has conditionally unstable atmosphere in a deep layer and the convective parameterization scheme employed has properties similar to one included in the QLM. It is well known that θ_e in the boundary layer increases as a tropical storm intensifies. Invoking parameterized convection at each time step will permit the development of a model convective cloud (cloud sounding through the current predicted value of θ_e in the boundary layer) and transfer of moisture and heat from low levels to upper troposphere, in a time to step at such a grid point (the temperature and mixing ratio at any point in the column will be adjusted according to the parameterization procedure). On the other hand, the transport of moisture and heat from low layers into the upper troposphere in a real cumulonimbus cloud takes place in several minutes; therefore the impact of increased θ_e in the boundary layer appears in the upper troposphere after several minutes. Accordingly, the time taken in a fine mesh model to vertically distribute heat and moisture due to convection is likely to be closer to that in nature, if either the convective parameterization (like one based on Kuo's work) is invoked at intervals of several time steps or a gradual vertical transfer of moisture and heat are incorporated in the parameterization procedure. Even an undiluted ascent of air from the boundary layer into the upper troposphere takes several minutes; therefore, θ_e in a real storm is likely to be greater in the boundary layer than in the upper troposphere, during the period in which θ_e in the boundary layer is increasing. This last feature is also simulated better when the (Kuo-type) parameterized convection is evaluated at intervals of several time

steps than when it is evaluated at each time step (section 3). As noted above, storm intensity and motion in the present study are also simulated better in the former, than in the later, case.

Latent heating in a very deep column near the center becomes very vigorous, and much rapid intensification than observed occur when the parameterized convection is excluded (section 4). This last result and material discussed in the previous paragraph suggest that parameterized convective heating should be included in mesoscale models, but parameterization schemes that produce changes in the entire depth of model cloud concurrently should be invoked at intervals comparable to the time taken, in real convective clouds, to transport heat and moisture from low levels into the high troposphere.

References

Anthes, R.A., 1977, "A cumulus parameterization scheme utilizing a one-dimensional cloud model", *Mon. Wea. Rev.*, **105**, 270-286.

Arakawa, A., and Chen, W.H., 1987, "Closure assumption in the cumulus parameterization problem", Short and Medium Range Numerical Weather Prediction. T. Matsuno, Ed. Meteor. Soc. Japan, Universal Academy Press, 107-131.

Hong, S. Y., and Lee, D.K., 1994, "Numerical simulation of a meso- β scale heavy rainfall event over the Korean peninsula", Proc. AMS Conf. on Numerical Weather Prediction. Portland, Oregon., 245-247.

Janji'c, Z.I., 1990, "The step-mountain coordinate : Physical package", *Mon. Wea. Rev.*, **118**, 1429-1443.

Jones, R.W., 1986, "Mature structure and motion of a model tropical cyclone with latent heating by the resolvable scales", *Mon. Wea. Rev.*, **114**, 973-990.

Krishnamurti, T.N., Ramnathan Y., Pan, H.L., Pasch, R.J., and Molinari, J., 1980, "Cumulus parameterization and rainfall rates-I", *Mon. Wea. Rev.*, **111**, 465-472.

Kuo, H.L., 1965, "On formation and intensification of tropical cyclones through latent heat release by cumulus convection", *J. Atmos. Sci.*, **22**, 40-63.

Kuo, H.L., 1974, "Further studies of the parameterization of the influence of cumulus convection on large scale flow", *J. Atmos. Sci.*, **31**, 1232-1240.

Kuo, Y.H. and Anthes, R.A., 1984, "Semiprognostic tests of Kuo-type cumulus parameterization schemes in an extratropical system", *Mon. Wea. Rev.*, **112**, 1482-1497.

Mathur, M.B., 1983, "A quasi-Lagrangian regional model designed for operational weather prediction", *Mon. Wea. Rev.*, **111**, 2087-2098.

Mathur, M.B., 1991, "The National Meteorological Center's Quasi-Lagrangian Model for hurricane prediction", *Mon. Wea. Rev.*, **119**, 1419-1447.

Mathur, M.B., 1992, "Tropical storm motion and structure in a fine mesh primitive equation model", *Meteor. Atmos. Phys.*, **50**, 127-142.

Mathur, M.B. and Ruess, J., 1993, "Further evaluation of the Quasi-Lagrangian Model's forecast track guidance", *Mon. Wea. Rev.*, **121**, 1514-1530.

Mesinger, F., Black, T.L. and Janji'c, Z.I., 1988, "A summary of the NMC step mountain (ETA) coordinate model", Proc. Workshop on Limited-area Modeling Intercomparison. Boulder, NCAR, 91-98. [NCAR, P.O. Box 3000, Boulder, CO 80307.]

Molinari, J., and Dudek, M., 1992, "Parameterization of convective precipitation in mesoscale numerical models: A critical review", *Mon. Wea. Rev.*, **120**, 326-344.

NMC Development Division, 1988, "Documentation of the research version of the NMC Medium Range Forecast Model", [NMC Development Division, W/NMC2, WWB, Washington, DC 20233.]

Ooyama, K.V., 1982, "Conceptual evolution of the theory and modeling of the tropical cyclone", *J. Meteor. Soc. Japan*, **49**, 744-756.

Parrish, D.F., and Derber, J.C., 1992, "The National Meteorological Center's Spectral statistics-interpolation analysis system", *Mon. Wea. Rev.*, **120**, 1747-1763.

Phillips, N.A., 1979, "The Nested Grid Model", NOAA Technical Report NWS 22, Department of Commerce, 80 pp. [NOAA/NWS/NMC, Development Division, W/NMC2, WWB Room 204, Washington D.C. 20233.]

Reed, J.R., and Recker, E.E., 1971, "Structure and properties of synoptic-scale wave disturbances in the equatorial western Pacific", *J. Atmos. Sci.*, **28**, 1117-1133.

Rosenthal, S.L., 1978, "Numerical simulation of tropical cyclone development with latent heat release by the resolvable scales I: model description and preliminary results", *J. Atmos. Sci.*, **35**, 258-271.

Yamasaki, M., 1977, "A preliminary experiment of the tropical cyclone without parameterizing the effects of cumulus convection", *J. Met. Soc. Japan*, **55**, 11-30

Zhang, D.L., Hsie, E.Y. and Moncrieff, M.W., 1988, "A comparison of explicit and implicit prediction of convective and stratiform precipitating weather systems with a meso-β scale numerical model", *Q.J.R. Meteorol. Soc.*, **114**, 31-60.